Spectroscopy and analysis of radiative and nonradiative processes in Ti^{3+}:Al_2O_3 crystals

M. Grinberg
Institute of Physics, Nocholas Copernicus University, PL87-100 Torun, Poland

A. Mandelis
Photothermal and Optoelectronic Diagnostics Laboratory, Department of Mechanical Engineering, University of Toronto, Toronto Canada M5S 1A4 and Ontario Laser and Lightware Research Center, University of Toronto, Toronto, Canada

K. Fjeldsted
Crystar Research Corporation, Victoria, British Columbia, Canada

A. Othonos
Ontario Laser and Lightware Research Center, University of Toronto, Toronto, Canada
(Received 2 November 1992; revised manuscript received 19 April 1993)

Experimental spectroscopic and time-resolved luminescence measurements of the Ti^{3+}:Al_2O_3 crystalline system have been performed. The absorption and fluorescence spectra obtained have led to a reconsideration of prevailing theoretical models for the radiative relaxation process in Ti:sapphire crystals. A realistic, two-dimensional configuration-coordinate space model has been constructed to describe the Jahn-Teller distortion of the system. Consideration of the nonlinear contributions to the electron-lattice coupling potential was found to contribute little to the second luminescence emission maximum, thus indicating that the electron-phonon interaction is essentially linear in the ground state. The main effect of the nonlinearity was found to be in the value of the nonradiative activation energy. The spin-orbit coupling was also incorporated in the model and was shown to be responsible for the nonradiative transitions in Ti^{3+}:Al_2O_3, while the phonon structure of the ground ($^2T_2$) state of the system results from both spin-orbit and nonlinear coupling with the lattice.

I. INTRODUCTION

Since sapphire doped with Ti^{3+}, Ti:Al_2O_3, has been demonstrated as a solid-state tunable laser system,[1,2] efforts have been undertaken to investigate the energetic structure and the radiative as well as the nonradiative processes in this material.[3,4] The electronic structure of octahedraly coordinated Ti^{3+} is a closed shell plus one $3d$ electron.[5] The d-electron level splits (omitting the spin) in the crystal field into triply degenerate $^2T_2$ and doubly degenerate ^2E states.[6] Although the basic spectroscopic properties of Ti:sapphire have been known for 30 years,[7] there are still some controversies related to the influence of electron-lattice interaction on the absorption and emission line shape and the emission kinetics. It is known that the large, static, Jahn-Teller, E-symmetry lattice distortion of the system in the excited ^2E state is responsible for the emission-absorption Stokes shift[8] and also for the internal conversion-induced quenching of the fluorescence at high temperatures.[3,4] On the other hand, the simplified one-dimensional configuration-coordinate models proposed by Albers, Stark, and Huber[3] and Ryvik and Buoncristiani[4] cannot describe quantitatively the radiative as well as the nonradiative processes. For instance, the predicted value of activation energy for the nonradiative deexcitation of the system, E_{NR}, depends very strongly on input assumptions, especially the values of elastic constants in the ground and excited states. Assuming linear coupling with the lattice in both ground and excited states, Albers, Stark, and Huber obtained $E_{NR}=7786\ cm^{-1}$.[3] The assumption of greater elastic constant in the excited state (nonlinear coupling) yields $E_{NR}=11\,826\ cm^{-1}$.[4] Taking into account the rapid decrease of the emission lifetime at temperatures above 300 K,[3-5] these values seem to be too large.

The aim of this paper is the detailed analysis of radiative and nonradiative transitions in Ti^{3+} in sapphire. Based on the spectroscopic data (absorption, emission, and fluorescence kinetics), we formulate an empirical configuration-coordinate model of the Ti^{3+} ion in an Al_2O_3 host, presented in Secs. III and IV. Our approach differs significantly from previous approaches[3,4] since we considered a more realistic two-dimensional configuration-coordinate space for describing the Jahn-Teller distortion of the system. Moreover, following Bill,[9] who considered the contributions of unharmonicity and second-order coupling terms to the excited ^2E state, we also consider the nonlinear contributions to the electron-lattice coupling. Furthermore, owing to its importance to nonradiative transitions, we also discuss the second-order coupling term in the case of the $^2T_2$ ground state. This paper addresses mainly radiative transitions. In the companion paper,[10] the detailed analysis of nonradiative processes is presented.

0163-1829/93/48(9)/5922(13)/$06.00

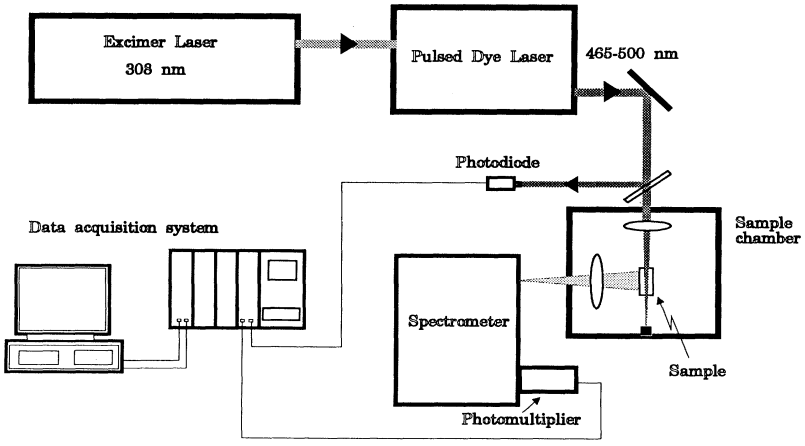

FIG. 1. Experimental setup for time-resolved fluorescence measurements of Ti^{3+}:Al_2O_3 crystal samples. See text for details.

II. EXPERIMENTAL TECHNIQUE

The experimental setup utilized in the time-resolved fluorescence measurements of the crystal sample is shown in Fig. 1. As seen from the schematic, the main pump laser was a pulsed excimer laser (model Heperex 400, Lumonics), which was set to lase at 308 nm (XeCl). This laser was generating pulses approximately 15 ns wide [full width at half maximum (FWHM)] at a repetition rate of 60 Hz and energies of 150 mJ/pulse. This excimer laser was used to pump a pulsed dye laser (model HyperDye 300, Lumonics) with a dye medium of Coumarin 480 (Exciton Chemical Co.). This dye dissolved in methanol allowed a tuning range of the dye laser between 465 and 500 nm and energies in excess of 15 mJ/pulse. The pulses coming out of the dye laser were measured to be approximately 10 ns wide. The laser beam out of the dye laser was directed in the sample chamber where it was focused through the sample with a long-focal-length lens (this allowed all the beam to pass through the crystal sample). Part of the laser beam, before it reached the chamber, was reflected onto a fast photodiode whose signal was used to trigger the data-acquisition system. In the sample chamber, the fluorescence from the sample was collected with a lens and directed into a spectrometer and, finally, onto a photomultiplier. The signal from the photomultiplier was fed into a gated integrator and boxcar averager (model SR250, Stanford Research Systems Inc.) and then into a computer through a computer interface module (model SR245). In this manner the luminescent decay of our crystal was measured to be purely exponential, as expected, with a metastable state lifetime $\tau = 3.85$ μs. Ti:sapphire absorption spectra in the 300–700-nm region were obtained using a spectrophotometer in the standard transmission mode.

The broadband fluorescence spectra from the sample were obtained using a similar experimental setup (see Fig. 2). However, the source of excitation was a cw argon-ion laser generating 1.5 W average energy at 488 nm. Just as in the time-resolved measurements, the laser beam was directed into the sample chamber where a lens was utilized to collect the fluorescence signal from the sample. The fluorescent light was then directed through a spectrometer and finally into a silicon detector. The signal from the detector was synchronized with the spectrometer wavelength setting through a computer data-acquisition hardware and software. This synchronization made intensity measurements of fluorescence as a function of wavelength possible.

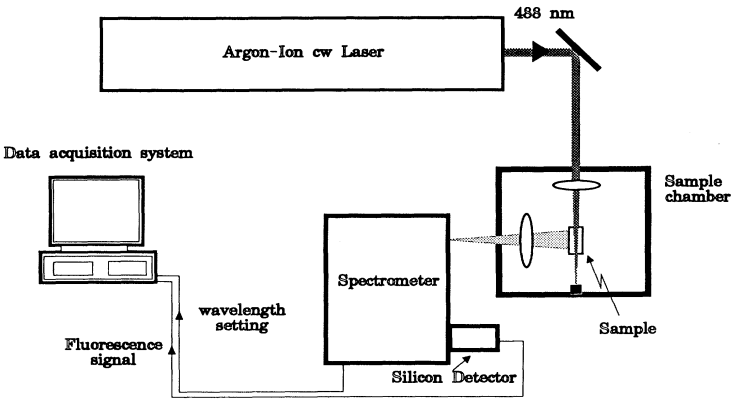

FIG. 2. Experimental setup for fluorescence spectra acquisition of Ti^{3+}:Al_2O_3 crystal samples. See text for details.

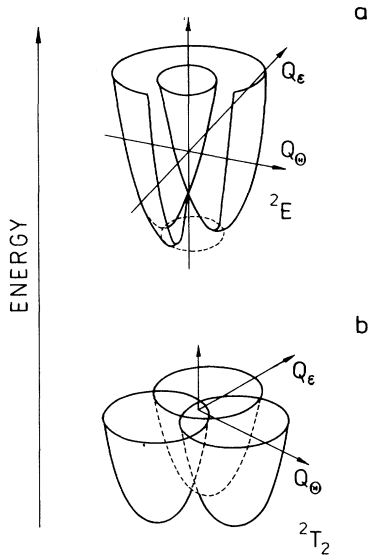

FIG. 3. Configuration-coordinate diagrams for Jahn-Teller effect. (a) E-electronic state and E-symmetry distortion; (b) T_2-electronic state and E-symmetry lattice distortion. Q_ε and Q_θ represent the normal coordinates related to E-symmetry distortion.

III. BASIC ASSUMPTIONS AND HAMILTONIAN OF THE SYSTEM

The octahedrally coordinated Ti^{3+} ions in sapphire compose a system wherein a d^1 electron is in a ^2E excited or $^2T_2$ ground state.[6] We have assumed that the dominant lattice distortion has E symmetry, and so the electron-phonon interaction causes the Jahn-Teller splitting of both ^2E and $^2T_2$ states. The typical configuration-coordinate diagrams for both cases are presented qualitatively in Fig. 3.[11]

To consider also the possibility of nonradiative transitions, we have performed calculations including the spin-orbit interaction in the electronic part of the Hamiltonian. It has been postulated[10] that the spin-orbit coupling of the Γ_8 component of the $^2T_2$ ground state with ^2E excited state is responsible for the radiationless deexcitation of Ti^{3+}. The spin-orbit interaction is also important as long as one is interested in the splitting of the zero-phonon line and the phonon structure of the ground state.

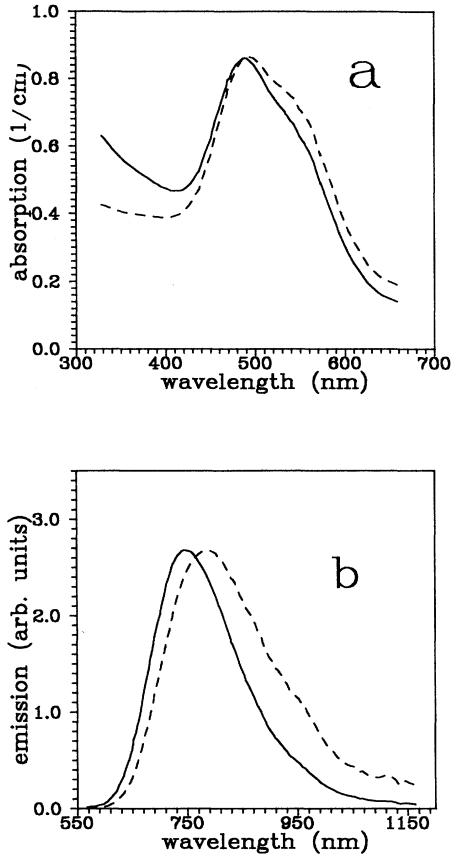

FIG. 4. (a) Absorption and (b) fluorescence spectra for Ti^{3+}:sapphire. Solid curves correspond to the experimental emission and absorption spectra; dashed curves correspond to the calculated spectral line shapes.

To perform detailed calculations, we have analyzed the absorption (transmission) and fluorescence spectra of Ti^{3+} (see Fig. 4). We have assumed that the positions of the maxima of the absorption and fluorescence correspond to the Frank-Condon transitions (transitions without changing the value of the configuration coordinate). The absorption coefficient $\mu(\hbar\Omega)$ and the emission intensity $I(\hbar\Omega)$ are related to the line shape of the spectrum, which, in our case, is defined by vibronic overlaps $I_{\text{vib}}(\hbar\Omega)$ as follows:[12]

$$\mu(\hbar\Omega) \propto I_{\text{vib}}(\hbar\Omega)\hbar\Omega \ , \tag{1}$$

TABLE I. Maxima in the absorption and emission spectra of $Ti:Al_2O_3$.

					Present work	
Absorption (cm^{-1})	Refs. 13,8,5	Ref. 3	Ref. 4	Ref. 7	Intensity	Line shape
$\hbar\Omega_1$	20 476	20 618	20 600	20 300	20 492	20 366
$\hbar\Omega_2$	17 987	18 182			18 180	18 180[a]
Emission (cm^{-1})						
$\hbar\Omega_3$	14 380	13 158	13 333		13 387	12 740

[a]Since the absorption line shape differs only little from the absorption coefficient, we assumed the same position of the second absorption maximum for the line shape and the absorption coefficient.

$$I(\hbar\Omega) \propto (\hbar\Omega)^4 I_{\text{vib}}(\hbar\Omega) \ . \tag{2}$$

Here Ω is the frequency of the absorbed-emitted photon. Since the Frank-Condon rule concerns the vibronic line shape rather than the absorption coefficient and emission intensity, we have calculated the spectral line shapes first according to Eqs. (1) and (2), and then we used the energies of their maxima as input parameters for calculations of configuration-coordinate diagrams. The respective data are listed in Table I. We have used an empirical approach in which matrix elements of the electronic part of the Hamiltonian of the system have been scaled to the energies of the Frank-Condon transitions with free parameters defined by the matrix elements of the electron-phonon interaction Hamiltonian.

The total Hamiltonian of the system is given by

$$H(q,Q)=H_e(q)+H_l(Q)+H_{e\text{-}l}(q,Q) \ , \tag{3}$$

where $H_e(q)$, $H_l(Q)$, and $H_{e\text{-}l}(q,Q)$ are the electronic, vibronic, and electron-phonon interaction Hamiltonians, respectively. q and Q correspond to electronic and ionic coordinates, respectively. The lattice Hamiltonian can be approximated by the harmonic term and is given by

$$H_l=\frac{1}{2}\sum_i Q_i^2 \ . \tag{4}$$

The electron-phonon interaction Hamiltonian can be obtained by considering the changes of total potentials related to ionic motion. One obtains

$$H_{e\text{-}l}=\sum_i \left[\frac{\partial V(q,Q)}{\partial Q_i}\right] Q_i+\frac{1}{2}\sum_{ij}\frac{\partial^2(q,Q)}{\partial Q_i \partial Q_j} Q_i Q_j + O(Q_i Q_j Q_k) \ . \tag{5}$$

In Eqs. (4) and (5), Q is in units of $(\hbar/M\omega)^{1/2}$, where M is the reduced mass of the ions involved. The phonon energy is given in units of $\hbar\omega$. However, it should be mentioned that $\hbar\omega$ is only the unit of energy, and since our vibration problem is not a simple one-dimensional harmonic oscillator and we assume nonlinear coupling with lattice vibrations, $\hbar\omega$ may not be equal to the phonon energy. i and j label the normal configuration coordinates. In the case of the E mode, we have two independent configurational coordinates: Q_θ and Q_ε. It should also be mentioned that, included in the second-order contributions in Eq. (5), we consider the changes of the elastic constant of the medium as related to the various electronic rearrangements when the system is in different electronic states. We also consider the spin-orbit interaction, and thus it is useful to use the total angular momentum wave-function basis $\{\phi_j^\Gamma\}$, where n corresponds to the irreducible representation of the crystal symmetry point group and J is the total angular momentum quantum number. The relations between the $\{\phi_j^\Gamma\}$ and the crystal-field basis functions can be obtained using the Clebsch-Gordon coefficients. For the case of octahedral symmetry (O_h point group) the coefficients are listed in Tables II and III.[14]

TABLE II. Clebsch-Gordon coefficients for the ^2E state ($u=(3z^2-r^2)/2$, $v=3^{1/2}(x^2-y^2)/2$, crystal-field basis).

^2E	$u_{-1/2}$	$u_{1/2}$	$v_{-1/2}$	$v_{1/2}$
$\phi^8_{-3/2}$	0	0	0	1
$\phi^8_{-1/2}$	1	0	0	0
$\phi^8_{1/2}$	0	−1	0	0
$\phi^8_{3/2}$	0	0	−1	0

Considering that the above-mentioned interactions in Eq. (3) do not remove the Kramers degeneracy, one takes into account two functions for the ^2E and three functions for the ^2T state. Thus the electronic part of the Hamiltonian in the angular momentum wave-function representation has the form

$$H_e=\begin{pmatrix} E_{^2E} & 0 & 0 & \sqrt{3}/\sqrt{2}\beta & 0 \\ 0 & E_{^2E} & 0 & 0 & \sqrt{3}/\sqrt{2}\beta \\ 0 & 0 & E_{^2T_2}+\beta & 0 & 0 \\ \sqrt{3}/\sqrt{2}\beta & 0 & 0 & E_{^2T_2}-\beta/2 & 0 \\ 0 & \sqrt{3}/\sqrt{2}\beta & 0 & 0 & E_{^2T_2}-\beta/2 \end{pmatrix} . \tag{6}$$

Here β is the spin-orbit coupling constant.[6] Since $E_{^2E}$ and $E_{^2T_2}$ correspond to zero-phonon energies of the excited and

TABLE III. Clebsch-Gordon coefficients for $^2T_2$ state ($\xi=yz$, $\eta=zx$, $\zeta=xy$, crystal-field basis).

$^2T_2$	$\xi_{-1/2}$	$\xi_{1/2}$	$\eta_{-1/2}$	$\eta_{1/2}$	$\zeta_{-1/2}$	$\zeta_{1/2}$
$\phi^7_{-1/2}$	0	$-i/\sqrt{3}$	0	$1/\sqrt{3}$	$i/\sqrt{3}$	0
$\phi^7_{1/2}$	$-i/\sqrt{3}$	0	$1/\sqrt{3}$	0	0	$-i/\sqrt{3}$
$\phi^8_{-3/2}$	$-i/\sqrt{6}$	0	$1/\sqrt{6}$	0	0	$i\sqrt{2}/\sqrt{3}$
$\phi^8_{-1/2}$	0	$i/\sqrt{2}$	0	$-1/\sqrt{2}$	0	0
$\phi^8_{1/2}$	$-i/\sqrt{2}$	0	$-1/\sqrt{2}$	0	0	0
$\phi^8_{3/2}$	0	$i/\sqrt{6}$	0	$1/\sqrt{6}$	$i\sqrt{2}/\sqrt{3}$	0

ground states, respectively, the lattice Hamiltonian should include the Jahn-Teller stabilization energies $E_{JT}(E)$ and $E_{JT}(T)$ for the excited and ground states, respectively.[15] This gives the diagonal components of H_l:

$$H_l \begin{bmatrix} E \\ T \end{bmatrix} = E_{JT} \begin{bmatrix} E \\ T \end{bmatrix} + \frac{1}{2}(Q_\theta^2 + Q_\varepsilon^2) \ . \tag{7}$$

Since E-symmetry distortion does not mix the E and T_2 electronic states, the electron-phonon interaction Hamiltonian matrix element of arbitrary components, the first of the ^2E state and the second of the $^2T_2$ state, is zero. Thus the electron-phonon Hamiltonian is represented by a diagonal block matrix with a 2×2 matrix for the ^2E and a 3×3 matrix for the $^2T_2$ state:

$$H_{e\text{-}l}(^2E) = L_E \begin{bmatrix} -Q_\theta & -Q_\varepsilon \\ -Q_\varepsilon & Q_\theta \end{bmatrix} + K_E \begin{bmatrix} \frac{1}{2}(Q_\theta^2 - Q_\varepsilon^2) & -Q_\theta Q_\varepsilon \\ -Q_\theta Q_\varepsilon & -\frac{1}{2}(Q_\theta^2 - Q_\varepsilon^2) \end{bmatrix} \tag{8}$$

and

$$H_{e\text{-}l}(^2T_2) = L_T \begin{bmatrix} 0 & \sqrt{2}Q_\varepsilon & -\sqrt{2}Q_\theta \\ \sqrt{2}Q_\varepsilon & Q_\theta & -Q_\varepsilon \\ -\sqrt{2}Q_\theta & -Q_\varepsilon & -Q_\theta \end{bmatrix} + K_T \begin{bmatrix} 0 & \sqrt{2}Q_\varepsilon Q_\theta & (Q_\theta^2 - Q_\varepsilon^2)/\sqrt{2} \\ \sqrt{2}Q_\varepsilon Q_\theta & -(Q_\theta^2 - Q_\varepsilon^2)/2 & -Q_\varepsilon Q_\theta \\ (Q_\theta^2 - Q_\varepsilon^2)/\sqrt{2} & -Q_\varepsilon Q_\theta & (Q_\theta^2 - Q_\varepsilon^2)/2 \end{bmatrix} . \tag{9}$$

Here:[11]

$$\begin{aligned} &L_E = \frac{1}{2}\left[-\left\langle u \left| \frac{\partial V}{\partial Q_\theta} \right| u \right\rangle + \left\langle v \left| \frac{\partial V}{\partial Q_\varepsilon} \right| v \right\rangle \right], \quad K_E = -\frac{1}{2}\left[\left\langle u \left| \frac{\partial^2 V}{\partial Q_\theta^2} \right| u \right\rangle + \left\langle v \left| \frac{\partial^2 V}{\partial Q_\theta^2} \right| v \right\rangle \right] , \\ &L_T = \frac{1}{2}\left\langle \zeta \left| \frac{\partial V}{\partial Q_\theta} \right| \zeta \right\rangle, \quad K_T = \frac{1}{2}\left[\left\langle \zeta \left| \frac{\partial^2 V}{\partial Q_\theta^2} \right| \zeta \right\rangle - \left\langle \zeta \left| \frac{\partial^2 V}{\partial Q_\varepsilon^2} \right| \zeta \right\rangle \right] . \end{aligned} \tag{10}$$

IV. CALCULATIONS

The spin-orbit coupling significantly changes the electronic manifold energies only for the region where configurational surfaces cross over or are close to one another. Therefore, since the minima of the configuration energies of the ^2E and $^2T_2$ states are well separated by an energy equal to the zero-phonon line transition, $-\Delta E = 16\,200\ \text{cm}^{-1}$, the values of the parameters $L_E[E_{JT}(E)]$, $L_T[E_{JT}(T)]$, K_E, and K_T can be obtained assuming $\beta=0$. Actually, performing calculations assuming $\beta=0$ and $200\ \text{cm}^{-1}$, we have found the differences between the values of these parameters were less than 1%. By omitting the spin-orbit interaction, we can get compact, analytical expressions. Therefore we present here only the formulas obtained using this simplification. Furthermore, we present the configuration-coordinate diagrams obtained using the electron-phonon coupling defined by constants L_E, L_T and K_E, K_T calculated under the assumption $\beta=0$ and including the nonzero spin-orbit coupling given by the Hamiltonian [Eq. (6)]. Using Eqs. (7)–(9), one can calculate the Jahn-Teller stabilization energies.[9] The results are

$$E_{JT}(E) = \tfrac{1}{2}L_E^2/(1-K_E) \tag{11}$$

and

$$E_{JT}(T) = 2L_T^2/(1+2K_T) \ . \tag{12}$$

To consider the positions of the energy minima on the Q_θ, Q_ε plane, one can use the new coordinate set (α and ρ) defined by

$$Q_\theta/Q_\varepsilon = \cot\alpha \tag{13}$$

and

$$\rho = (Q_\theta^2 + Q_\varepsilon^2)^{1/2} \ . \tag{14}$$

For the ^2E state, one obtains three equivalent minima at the positions

$$\rho = L_E/(1-K_E) \quad \text{and} \quad \alpha = \pi/3,\ \pi, \text{ and } 5\pi/3 \ . \tag{15}$$

In addition, three saddle points, characterized by the relaxation energy $\frac{1}{2}L_E^2/(1+K_E)$, are placed at

$$\rho = L_E/(1+K_E) \quad \text{and} \quad \alpha = 0,\ 2\pi/3, \text{ and } 4\pi/3 \ . \tag{16}$$

It is evident that the minima become the saddle points and vice versa if K_E becomes negative. For the $^2T_2$ state, we have three minima placed at

$$\rho = L_T/(1+2K_T) \quad \text{and} \quad \alpha = 0,\ 2\pi/3, \text{ and } 4\pi/3 \ . \tag{17}$$

It has been found that in order to fit the configuration-coordinate diagram to the experimental Frank-Condon transitions, we had to assume that the minima of the ground state are placed under the saddle points of the excited state. The configuration-coordinate diagrams can be calculated via the roots of

$$\det|H(Q) - E| = 0 \ , \tag{18}$$

where $H(Q)$ is the total Q-dependent Hamiltonian given by the sum of Eqs. (6) and (7) and the block matrices given by Eqs. (8) and (9).

We fitted the values of parameters of the configuration-coordinate diagrams considering the absorption and emission spectral line shapes. We have two maxima in the absorption spectra corresponding to the Frank-Condon transitions from the minimum of the ground state to two components of the excited state. Choosing the zero energy at a minimum of energy of the $^2T_2$ electronic manifolds and considering a particular minimum of energy of the $^2T_2$ state—for instance, one corresponding to $\rho=2L_T/(1+2K_T)$ and $\alpha=0$ (or one can consider another equivalent minimum [see conditions (17)] and obtain the same results)—one obtains two equations:

$$\hbar\Omega_1=E_+ , \tag{19}$$

$$\hbar\Omega_2=E_- . \tag{20}$$

Here $\hbar\Omega_1$ and $\hbar\Omega_2$ (listed in Table I) are the energies of photons corresponding to the transitions to upper (+) and lower (−) component of the excited state:

$$E_\pm=\tfrac{1}{2}L_E^2/(1-K_E)+2L_T^2(1\pm K_E)/(1+2K_T) \mp 2L_EL_T/(1+2K_T)+\Delta E . \tag{21}$$

ΔE is the energy of the zero-phonon line deduced from the experimental spectra: $\Delta E=16\,200$ cm^{-1}. A third equation can be obtained from the fluorescence maximum $\hbar\Omega_3=12\,740$ cm^{-1}. This band corresponds to the Frank-Condon transition from the minimum of the excited state with energy ΔE placed at $\rho=L_E/(1-K_E)$ and $\alpha=\pi$ [or any other equivalent point; see conditions (15)] with respect to the ground state. Thus the third equation has the form

$$\hbar\Omega_3=\Delta E-E_g , \tag{22}$$

where the energy of the ground state is given by

$$E_g=2L_T^2/(1+2K_T)+\tfrac{1}{2}(1-K_T)[L_E/(1-K_E)]^2 - L_TL_E/(1-K_E) . \tag{23}$$

It is seen that we have three equations [(19), (20), and (22)] and four free parameters L_E, K_E, L_T, and K_T. Therefore the value of one of those should be obtained in some other way. Here we discuss the value of K_T. Formally, the value of K_T can be calculated if one knows the potential energy in the vicinity of the minimum of the $^2T_2$ manifold. Considering the particular minimum at $Q_\theta=2L_T/(1+2K_T)$, $Q_\varepsilon=0$, one can obtain the potential energy in the form

$$V(Q)=V[Q_\theta=2L_T/(1+2K_T),Q_\varepsilon=0]+\tfrac{1}{2}(1+2K_T)[Q_\theta-2L_T/(1+2K_T)]^2+\tfrac{1}{2}(1-2K_T)Q_\varepsilon^2 . \tag{24}$$

Gachter and Koningstein[8] have recognized two different phonon energies in the ground state of Ti^{3+}:Al_2O_3: $\hbar\omega_{g1}=257$ cm^{-1} and $\hbar\omega_{g2}=220$ cm^{-1}. Assuming that $g1$ corresponds to the ε mode and $g2$ to the θ mode or vice versa, Eq. (24) allows the calculation of the absolute value of K_T (=0.077) and of the average phonon energy in the ground state ($\hbar\omega_g=239$ cm^{-1}). This is the phonon energy under the assumption of linear coupling, i.e., $K_T=0$. Although this result seems to be reasonable, it may be fairly incorrect, given that spin-orbit coupling can also cause the splitting of phonon modes (see the Appendix). Therefore, in this work, we cover all possibilities and present the configuration-coordinate diagrams for $K_T=0.077$, $K_T=-0.077$, $K_T=0$, and $K_T=-0.043$. The first two cases correspond to the situation when the phonon energy "splitting" is related only to the nonlinear electron-lattice coupling and the third case when it is related only to the spin-orbit interaction. The fourth case corresponds to the situation when the phonon energy "splitting" in the ground state depends on both effects. It should be mentioned here that the set of parameters related to $K_T=-0.043$ corresponds to the best reproduction of the fluorescence kinetics in Ti^{3+}:Al_2O_3 (see companion paper[10]).

Since L_E and $E_{JT}(E)$, and L_T and $E_{JT}(T)$ are pairwise directly related to each other by means of Eqs. (11) and (12), we calculated the Jahn-Teller stabilization energies and the K_E coefficient. The obtained values of the fitted parameters are listed in Table IV. The corresponding configuration-coordinate diagrams are presented in Fig. 5. Here the sections along Q_θ are presented with $Q_\varepsilon=0$. One can see the anticrossing behavior of the lower component of the ^2E state with the upper component of the $^2T_2$ state. In this region the electronic parts of the wave functions are well mixed. As has been suggested[10] that this effect is mainly responsible for the nonradiative deexcitation of Ti^{3+}. One can obtain the energy barrier for nonradiative transitions E_{NR}, measured as the energy of ^2E-$^2T_2$ "crossing" with respect to the minimum energy of the excited state. The other parameters which can be obtained are the stabilization energy of the excited state (the relative energy of the minima and saddle points, Δ_1) and the energy of the second fluorescence band with the maximum $-\hbar\Omega_4$ (energy of the transition between the minimum of the ^2E state and the upper component of the $^2T_2$ state; see Fig. 5). The second maximum in fluorescence is expected to appear when the system in the excited state is stabilized in an individual minimum, which is created due to the second-order contribution in the electron-phonon interaction Hamiltonian ($K_E\neq 0$).

In Fig. 6 the configuration-coordinate energies of the lowest components of the ^2E and $^2T_2$ states are presented as a function of Q_θ and Q_ε. Here the processes of absorption, relaxation, and fluorescence are shown.

It seems that positive K_T values are rather unphysical, since they cause a relatively low barrier for nonradiative

TABLE IV. Calculated spectroscopic parameters of $Ti:Al_2O_3$.

	K_T				
	0.077	−0.077	0	−0.043	Experiment
K_E	0.385	0.195	0.289	0.236	
$E_{JT}(E)$ (cm^{-1})	2879	2993	2909	2924	
$E_{JT}(E)$ (cm^{-1})	223	113	158	132	
Δ_1 (cm^{-1})	1605	966	1311	1125	
$\hbar\Omega$ (cm^{-1})	8401	11 830	10 351	11 225	above 10 500
E_{NR} (cm^{-1})	985	7171	2633	4507	
$\hbar\omega_1(^2E)$ (cm^{-1})	187	214	202	208	~200 (Ref. 3)
$\hbar\omega_2(^2E)$ (cm^{-1})	185	202	200	202	~200 (Ref. 3)

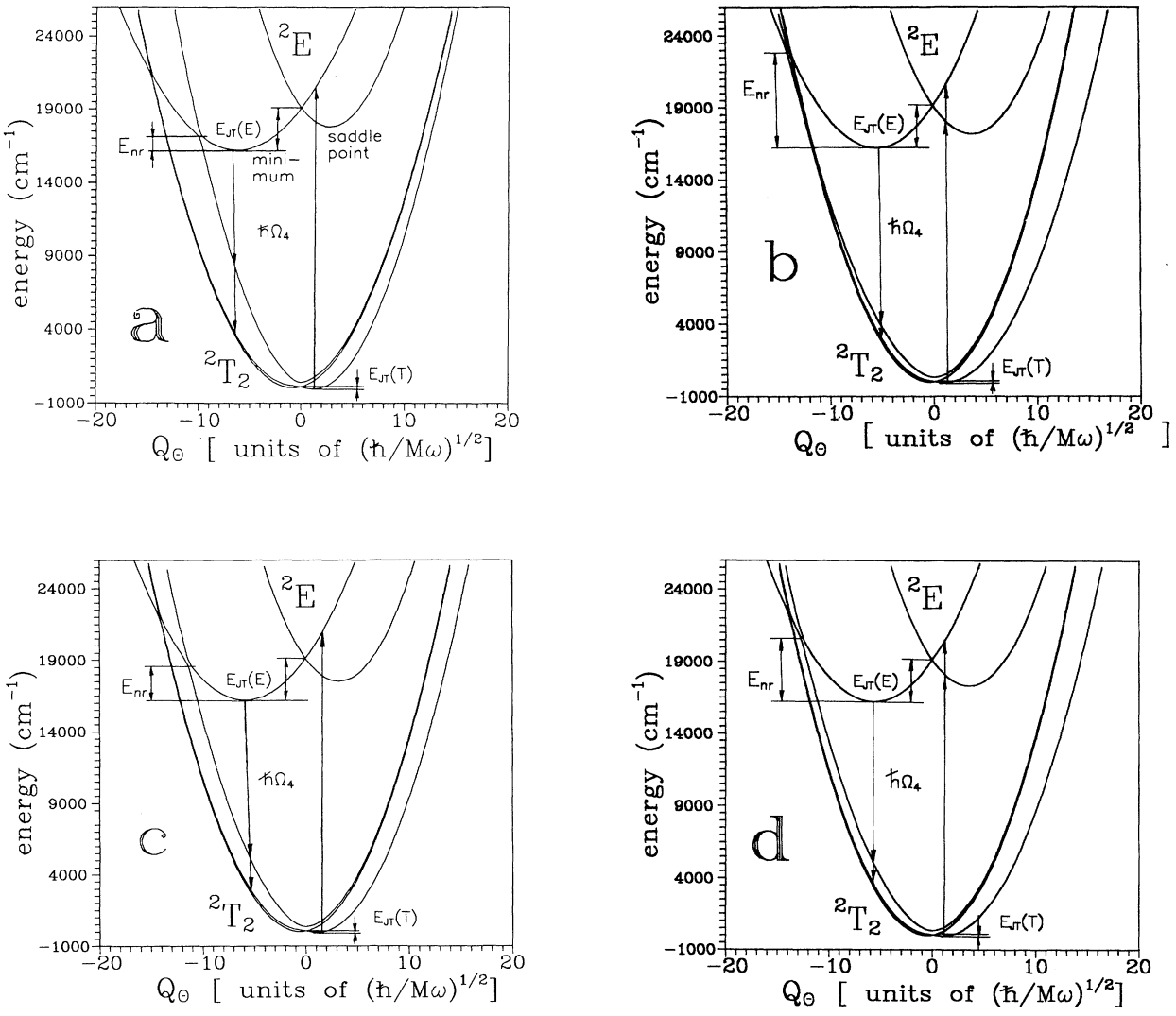

FIG. 5. Configuration-coordinate diagrams for Ti^{3+} for four different parameter sets fitted to the spectroscopic data. Here the section of configuration surfaces along Q_θ is presented assuming $Q_\varepsilon=0$: (a) for the parameter set generated by $K_T=0.077$, (b) for $K_T=-0.077$, (c) for $K_T=0$, and (d) for $K_T=-0.043$. To obtain these plots, the spin-orbit couplings have been assumed to be 200 cm^{-1}. The Frank-Condon transitions are indicated by arrows.

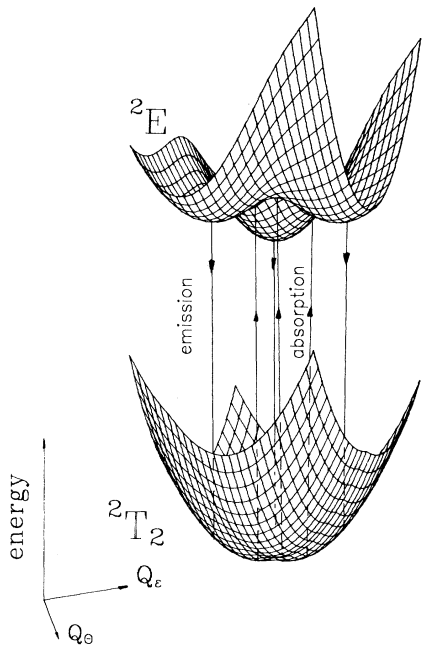

FIG. 6. Full configuration-coordinate diagrams for the lowest component of the $^2T_2$ state and lower component of the ^2E state. The Frank-Condon transitions are indicated by arrows.

transitions (985 cm^{-1}). Experimentally, small nonradiative transition rates for small and intermediate temperatures have been found. Usually, the nonradiative decay becomes important for temperatures greater than 300 K.[3-5] Negative and rather small K_T (with absolute value smaller than 0.077) is much more reliable, since it gives, in addition, a very good prediction of the energy of the second band in the emission spectra. An additional argument for small K_T is the specific structure of the first excited phonon state of the $^2T_2$ state obtained including only the spin-orbit coupling. For these reasons further calculations have been performed assuming $K_T=0$ and $K_T=-0.043$.

V. QUANTITATIVE ANALYSIS OF THE EMISSION LINE SHAPE

It was shown in the preceding section that the nonlinear coupling with the lattice vibration in the case of the Ti:sapphire system in the excited state (^2E state) causes the stabilization of the system at individual points on the configurational plane. This is the reason for which one can reproduce the fluorescence spectrum in a relatively simple way using a two-dimensional oscillator model. Being in the excited state, the system can be described by three individual two-dimensional oscillators with the minima of the energy at three points in the configurational plane [Eq. (15)]. Let us focus at the minimum placed at $Q_\theta^0(E)=-L_E/(1-K_E)$, $Q_\varepsilon^0(E)=0$. The potential energy around that minimum can be given as follows:

$$V^E(Q)=V^E(Q^0)+\frac{1}{2}\sum_{i,j}\left[\frac{\partial^2 V(Q)}{\partial Q_i \partial Q_j}\right]Q_i Q_j \ , \tag{25}$$

where $i=\theta,\varepsilon$ and $j=\theta,\varepsilon$. Neglecting the spin-orbit interaction, one obtains

$$V^E(Q)=V^E(Q^0)+\tfrac{1}{2}[(1-K_E)\theta^2+(\tfrac{1}{2}-\tfrac{9}{2}K_E^2+2K_E)\varepsilon^2] \ , \tag{26}$$

where

$$\theta=Q_\theta-Q_\theta^0(E) \ \text{ and } \ \varepsilon=Q_\varepsilon-Q_\varepsilon^0(E) \ . \tag{27}$$

Since $\partial^2 V/\partial Q_\theta \partial Q_\varepsilon=0$, the θ and ε variables are separable. Thus each minimum of the ^2E state can be characterized by two independent modes with energies $\hbar\omega_1(^2E)$ and $\hbar\omega_2(^2E)$.[16] The calculated energies of these modes are presented in Table IV. One can see that for each case the energies of phonons in the excited state are smaller than in the ground state and in good agreement with experiment.[3,8]

The lower states to which transitions are probable are given by three two-dimensional harmonic oscillators with the minima of energy at the points given by conditions (17). Assuming that the ground state is characterized by linear coupling with the lattice ($K_T=0$), one obtains the potential energy of such a system as follows:

$$V^T(Q)=\frac{1}{2}\sum_{i=1}^{3}(\theta_i^2+\varepsilon_i^2) \ , \tag{28}$$

where

$$\theta_i=Q_\theta-Q_{\theta i}^0(T) \ \text{ and } \ \varepsilon_i=Q_\varepsilon-Q_{\varepsilon i}^0(T) \ ; \tag{29}$$

i labels the minima.

This allows the calculation of the emission intensity $I(\hbar\Omega)$ using relation (2), where the vibronic reduction factor $I_{\text{vib}}(\hbar\Omega)$ corresponding to the line shape of the spectrum can be calculated from the expression

$$I_{\text{vib}}(\hbar\Omega)=\delta[\hbar\Omega-(\delta E-m\hbar\omega_g)] \times\sum_{i=i}^{3}\sum_{k=0}^{m}|\langle E^0\theta|T^k\theta_i\rangle|^2|\langle E^0\varepsilon|T^{m-k}\varepsilon_i\rangle|^2 \ . \tag{30}$$

If one takes into account the nonlinear coupling with the lattice in the ground state [see Eq. (24)], one should consider two different phonon energies $\hbar\omega_{g\varepsilon}$ and $\hbar\omega_{g\theta}$ related to ε and θ modes, respectively. Thus Eq. (30) can be recast in the new form

$$I_{\text{vib}}(\hbar\Omega)=\sum_{i=1}^{3}\sum_{k=0}^{3}\delta\{\hbar\omega-\Delta E+[k\hbar\omega_{g\theta_i}+(m-k)\hbar\omega_{g\varepsilon_i}]\} \times|\langle E^0\theta|T^k\theta_i\rangle|^2|\langle E^0\varepsilon|T^{m-k}\varepsilon_i\rangle|^2 \ . \tag{31}$$

Here δ is the Dirac delta function, $\langle E^0\theta|T^k\theta_i\rangle$ and $\langle E^0\varepsilon|T^{m-k}\varepsilon_i\rangle$ are the overlap integrals of the vibronic functions in the ^2E and $^2T_2$ states, k, $m-k$ are vibronic quantum numbers, i labels the components of the ground

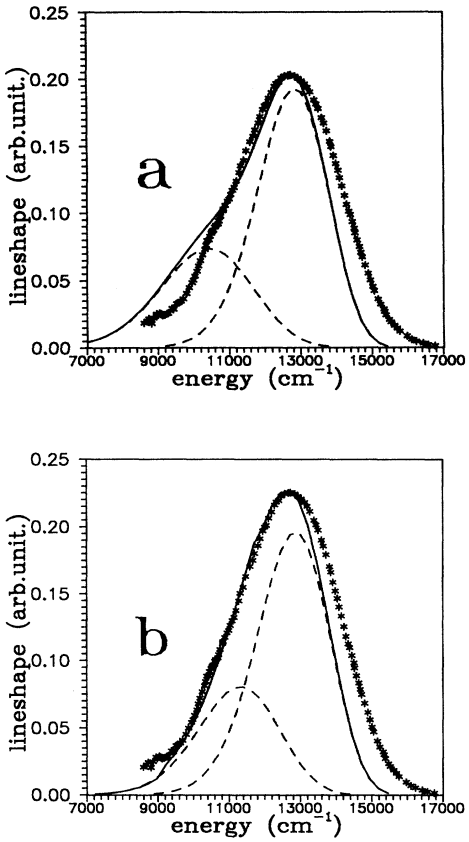

FIG. 7. Vibronic overlap spectral line shape for the emission spectrum of Ti^{3+} in Al_2O_3. Dashed curves correspond to the components of the spectrum; the solid line corresponds to the resulting line shape. Asterisks correspond to the experimental line shape at room temperature. (a) Calculations performed for two-dimensional oscillators defined by parameter set corresponding to $K_T=0$; (b) calculations performed for oscillators defined by parameter set corresponding to $K_T=-0.043$ (see Table IV). In both cases the reproduced line shapes have been normalized to the maximum in the experimental emission spectral line shape.

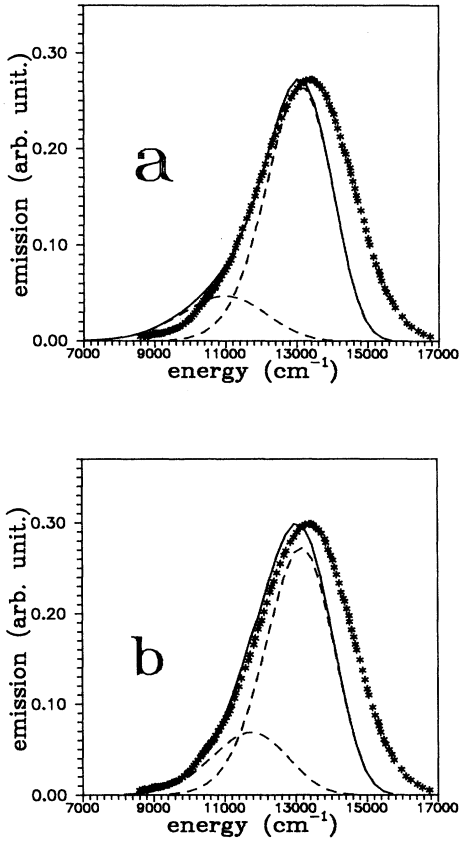

FIG. 8. Reproduced emission spectrum for Ti^{3+} in Al_2O_3. Dashed curves correspond to the components of the spectrum; the solid curve corresponds to the resulting intensity. Asterisks correspond to the experimental emission intensity. (a) corresponds to results obtained assuming $K_T=0$; (b) $K_T=-0.043$.

($^2T_2$) state (the minima of the potential energies), and $\hbar\omega$ is the energy of the emitted photons.

Since the vibronic wave functions $|E\rangle$ and $|T\rangle$ are harmonic-oscillator wave functions, the overlap integral can be calculated by the Manneback recurrence formulas.[17] For performing calculations the one value of the phonon energy in the ground state, $\hbar\omega_g=239$ cm,$^{-1}$ the same for the θ and ε modes, has been taken for $K_T=0$, whereas $\hbar\omega_{g\varepsilon}=249$ cm^{-1}, $\hbar\omega_{g\theta}=229$ cm^{-1} (Ref. 10) have been used to reproduce the spectrum for $K_T=-0.043$. The results of the calculations are presented in Figs. 7 and 8. In Fig. 7 the emission line shapes $I_{\rm vib}(\hbar\Omega)$ are presented. In Fig. 8 the emission intensities are calculated according to relation (2). One can see from Fig. 8 that for both sets of parameters there is a pronounced redshift of the calculated main maximum of the emission intensity with respect to the experimental spectrum. In fact, the spectra have been fitted using the Frank-Condon rule for the spectral line shape. Since the experimental line shape is significantly broader than the theoretical one, the respective shifts of the maxima of the emission intensity must be different (the shift for a broader line shape is greater). This effect is related to temperature: The calculations have been performed for 0 K, whereas the spectrum has been measured at 300 K. It is also possible to reproduce the spectra for any reasonable temperature by considering the emission from higher vibronic levels of the ^2E electronic state. Considering the Boltzmann occupation of the vibronic levels, one can calculate $I_{\rm vib}(\hbar\Omega,T)$ according to the formula

$$I_{\rm vib}(\hbar\Omega,T)=\sum_n S(n,T)\sum_{i=1}^{3}\sum_{k=0}^{m}\sum_{t=0}^{n}\delta\{\hbar\Omega-\Delta E+[k\hbar\omega_{g\theta_i}+(m-k)\hbar\omega_{g\varepsilon_i}-n\hbar\omega_e]\}$$
$$\times|\langle E^t\theta|T^k\theta_i\rangle|^2|\langle E^{n-t}\varepsilon|T^{m-k}\varepsilon_i\rangle|^2\ , \qquad (32)$$

where the Boltzmann occupation factor $S(n,T)$ is given by

$$S(n,T)=\exp(-n\hbar\omega_e/kT)\Big/\left[\sum_{n'}\rho(n')\exp(-n'\hbar\omega_e/kT)\right], \tag{33}$$

where n,n',t are the vibronic quantum numbers of the excited electronic state and $\rho(n')=(n'+1)$ is the density of states.[10] To obtain Eqs. (32) and (33), we have assumed the same phonon energy $\hbar\omega_e$ for both modes (ε and θ) in the excited state. For calculations, $\hbar\omega_e=201$ and 205 cm^{-1} have been taken for $K_T=0$ and -0.043, respectively. The emission spectra reproduced for $T=300$ K are presented in Fig. 9. Figure 9(a) presents the results obtained assuming $K_T=0$. Figure 9(b) presents the results obtained assuming $K_T=-0.043$. One can see that the correspondence between the theoretical results and experiment is quite good in both cases (slightly better for $K_T=-0.043$).

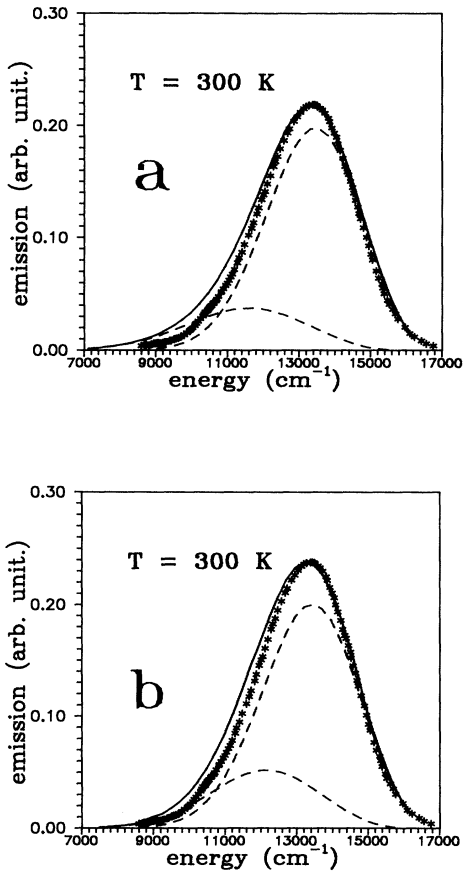

FIG. 9. Reproduced emission spectrum at room temperature. Dashed curves correspond to the components of the spectrum; the solid curve corresponds to the resulting intensity. Asterisks correspond to the experimental emission intensity. (a) corresponds to results obtained assuming $K_T=0$; (b) $K_T=-0.043$.

VI. COMPARISON WITH THE RESULTS OF OTHER MODELS AND CONCLUSIONS

Albers, Stark, and Huber[3] used the single-configuration-coordinate model for describing the nonradiative transition in Ti^{3+} in an Al_2O_3 host. However, the base model used by those authors was the two-configuration-coordinate model.[18] That model includes only the linear terms of electron-phonon interaction. In that case the system in the ^2E state is not stabilized at particular Q_θ and Q_e [see Fig. 3(a)], and therefore the second fluorescence band does not exist. Albers, Stark, and Huber have obtained the Huang-Rhys energy $S\hbar\omega=4410$ cm^{-1}. This quantity corresponds to $E_{JT}(E)+E_{JT}(T)$ in our model. The second quantity which one can deduce from Ref. 3 is $E_{NR}=7787$ cm^{-1}. These values for $S\hbar\omega$ and E_{NR} are greater than those obtained in the framework of our model. This results directly from the assumption of linear coupling with phonons in the ^2E state performed in Ref. 3. In this paper we have shown that nonlinear coupling yields smaller phonon energy in the excited state. This effect has been observed by Gachter and Koningstein,[8] but also by Albers, Stark, and Huber.[3] The second model, which has been published by Ryvik and Buoncristiani,[4] is the single-configuration-coordinate model. They postulated that the elastic constant in the excited state is greater than in the ground state. This assumption produces a much higher, unrealistic, energy barrier for nonradiative transitions: $E_{NR}=11\,826$ cm^{-1}. Our model predicts E_{NR} between 985 and 7171 cm^{-1}, depending on the second-order contribution to the electron-lattice coupling in the ground state.

The estimated value of K_E ($K_E=0.195-0.395$; Table IV) suggests that the second-order contribution to the electron-phonon interaction plays an important role when the system is in the ^2E state. In general, nonzero K_E causes stabilization of the system for particular ion displacements. The displacements of ions corresponding to configuration coordinates in the particular point on the θ,ε plane are presented in Fig. 10.[15] It is seen that the positions of the ions for the minimum energy of the system in the excited state correspond to the stress of the octahedron along one of the axes (x, y, or z). On the other hand, being in the ground state, the system reaches the minimum energy for the octahedron spread along adequate axes (x, y, or z).

It is interesting to consider whether the second-order terms in the electron-phonon interaction Hamiltonian also play an important role for the system in the ground state. The predicted energy of the second maximum in the fluorescence band obtained using only the linear term or a very small second-order term for the ground state is quite accurate. Therefore it seems that the electron-phonon interaction is almost linear in the ground state.

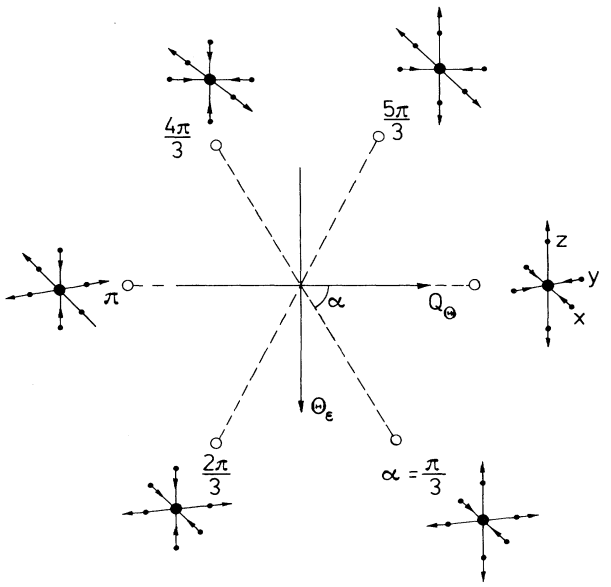

FIG. 10. Octahedron distortions and corresponding directions in the Q_θ, Q_ε plane. Open circles correspond to the positions of the minima and to the saddle points of the configuration energies. Adequate distortions of the octahedron consisting of the central Ti^{3+} ion and ligands are graphically presented near each point.

The two different phonons in the ground state are related to the nonlinear coupling with the lattice vibrations as well as the spin-orbit splitting of the $^2T_2$. Nevertheless, even very small nonlinearity of the electron-lattice interaction for the system in the ground state influences very effectively the value of the nonradiative activation energy (see Table IV and Fig. 5).

The spin-orbit coupling is important for two reasons: (a) It allows nonradiative transitions due to the mixing of the electronic parts of the wave functions of the ground and excited states.[10] (b) It yields the splitting of the $^2T_2$ state (the zero-phonon line as well as the phonon replica). It should be mentioned here that the value of the spin-orbit coupling parameter $\beta=200$ cm^{-1} used through out this paper is rather overestimated. The more reliable value $\beta=80$ cm^{-1} has been obtained from the spin-orbit splitting of the zero-phonon line of the ground state. Nevertheless, we have used this overestimated value to describe successfully the anticrossing behavior of the ^2E and $^2T_2$ states in configuration-coordinate diagrams.

ACKNOWLEDGMENT

The authors wish to gratefully acknowledge a Strategic Grant from the Natural Sciences and Engineering Research Council of Canada (NSERC), which made this work possible.

APPENDIX: PHONON STRUCTURE OF THE $^2T_2$ STATE IN Ti^{3+}:Al_2O_3

We have considered the phonon structure of the ground $^2T_2$ electronic manifold in Ti^{3+}:Al_2O_3 using an approach similar to the one proposed by Sturge[19] and Ham.[20] Actually, the case of Ti^{3+} $^2T_2$ zero vibronic state splitting has been discussed in a number of papers.[21–25] It is known that the trigonal crystal field and the spin-orbit interaction yield the splitting of the $^2T_2$ state into $_2E_{1/2}$, $_1E_{1/2}$, and $E_{3/2}$ Kramers doublets.[22] The effect of the $T\times\varepsilon$ Jahn-Teller distortion, which produces additional crystal field, is usually taken into account by considering the quenching of the electronic Hamiltonian matrix elements by the respective overlap integrals of the vibronic wave functions. A detailed analysis of the structure of the zero vibronic states has been performed by Macfarlane, Wong, and Sturge[23] and by Bates and Bentley.[24] These authors have obtained the "bare" electronic matrix elements related to the spin-orbit interaction (β) and the trigonal field (ν): $\beta=120$ cm^{-1} and $\nu=790$ cm^{-1} under the assumption of a medium Jahn-Teller effect in the $^2T_2$ state.[23] Since the analysis of the absorption and emission spectra presented in this work predicts rather small Jahn-Teller splitting of the ground state in the case of Ti^{3+}:Al_2O_3, we give here a more comprehensive analysis of the vibronic structure of the $^2T_2$ state. We have considered the zero vibronic states as well as the one-phonon excitation states related to the $^2T_2$ electronic manifold. Thus our basis consists of 18 adiabatic wave functions related to three electronic manifolds described by ξ, η, and ζ, which are represented as follows: $\varphi_\pm|0,0\rangle$, $\varphi_\pm|1,0\rangle$, and $\varphi_\pm|0,1\rangle$. φ is the electronic part of the wave function; ξ, η, and ζ (+ and − correspond to projection of the spin) and $|n,m\rangle$ are the vibronic wave functions corresponding to n and m phonon excitations related to the θ and ε modes, respectively. Considering that the perturbation Hamiltonian H' is given by the spin-orbit interaction $H_{\text{s.o.}}$ and the trigonal crystal field H_{trig}, one may calculate the nonvanishing, first-order matrix elements. Considering the electronic part of the wave functions, one obtains

$$\langle\xi_\pm|H'|\eta_\pm\rangle=\frac{\nu}{3}\pm i\frac{\beta}{2}\ , \tag{A1}$$

$$\langle\xi_\pm|H'|\zeta_\mp\rangle=\mp\frac{\beta}{2}\ , \tag{A2}$$

$$\langle\eta_\pm|H'|\zeta_\mp\rangle=i\frac{\beta}{2}\ , \tag{A3}$$

$$\langle\xi_\pm|H'|\xi_\pm\rangle=\langle\eta_\pm|H'|\xi_\pm\rangle=\frac{\nu}{3}\ . \tag{A4}$$

Here $\langle\ \rangle$ corresponds to integration over the electronic coordinate. Since the Jahn-Teller effect yields the splitting of the $^2T_2$ state in the configuration-coordinate space into ξ, η, and ζ electronic manifolds, each matrix element defined by (A1)–(A4) is quenched by the respective overlap integral related to the vibronic wave functions:

$$\gamma_{\alpha\alpha'}^{nn',mm'}=\alpha\langle\langle n,m|n',m'\rangle\rangle\alpha'\ . \tag{A5}$$

In Eq. (A5), $\langle\langle\ \rangle\rangle$ corresponds to integration over ionic (configuration) coordinates in two-dimensional space (θ and ε). In our case it is easy to obtain

$$\gamma_{\alpha\alpha'}^{00,00}=\exp(-S/2) \tag{A6}$$

for any α and α' and

$$\gamma_{\eta\xi}^{00,10}=\gamma_{\xi\xi}^{00,01}$$
$$=-\gamma_{\xi\eta}^{00,01}=-\gamma_{\xi\zeta}^{00,01}=-\frac{(3S)^{1/2}}{2}\exp(-S/2)\ , \tag{A7}$$

$$\gamma_{\eta\zeta}^{00,01}=\gamma_{\zeta\eta}^{00,01}=0\ , \tag{A8}$$

$$-\gamma_{\eta\xi}^{00,10}=\gamma_{\zeta\xi}^{00,10}$$
$$=\gamma_{\xi\eta}^{00,10}=-\gamma_{\xi\zeta}^{00,10}=\frac{S^{1/2}}{2}\exp(-S/2)\ , \tag{A9}$$

$$\gamma_{\eta\zeta}^{00,10}=\gamma_{\zeta\eta}^{00,10}=S^{1/2}\exp(-S/2)\ , \tag{A10}$$

$$\gamma_{\eta\xi}^{10,10}=\gamma_{\zeta\xi}^{10,10}=(1-S/4)\exp(-S/2)\ , \tag{A11}$$

$$\gamma_{\xi\eta}^{01,01}=\gamma_{\xi\zeta}^{01,01}=(1-3S/4)\exp(-S/2)\ , \tag{A12}$$

$$\gamma_{\eta\zeta}^{10,10}=(1-S)\exp(-S/2)\ , \tag{A13}$$

$$\gamma_{\eta\zeta}^{01,01}=\exp(-S/2)\ , \tag{A14}$$

$$\gamma_{\eta\zeta}^{01,10}=\gamma_{\eta\zeta}^{10,01}=0\ , \tag{A15}$$

$$\gamma_{\eta\xi}^{01,10}=-\gamma_{\zeta\xi}^{01,10}$$
$$=\gamma_{\xi\eta}^{01,10}=-\gamma_{\xi\zeta}^{01,10}=\frac{3^{1/2}}{4}S\exp(-S/2)\ . \tag{A16}$$

In Eqs. (A6)–(A16), S is the parameter related to the Jahn-Teller stabilization energy of the system in the $^2T_2$ state: $S=3E_{\rm JT}(T)/\hbar\omega$. The influence of coupling with higher excited vibronic states has been considered as a second-order perturbation. In the case of the Ti:sapphire, the corrections to the energy are given by diagonal terms:

$$M_{\alpha\alpha}^{(2)}=-\frac{1}{\hbar\omega}\left[\frac{\beta^2}{4}+\frac{\nu^2}{9}\right]\Gamma_{\alpha\alpha}^{ij}\ , \tag{A17}$$

where

$$\Gamma_{\alpha\alpha}^{ij}=\sum_{\alpha'\neq\alpha}\sum_{n>2}\sum_{k=0}\frac{|\langle\langle\alpha,i,j|\alpha',k,n-k\rangle\rangle|^2}{(n-2+i+j)}\ . \tag{A18}$$

In Eqs. (A17) and (A18), α' and α correspond to ξ, η, and ζ; i and j are the vibronic quantum numbers. The sums over the higher excited vibronic states in $\Gamma_{\alpha\alpha}^{ij}$ can be reduced as follows:

$$\Gamma_{\alpha\alpha}^{00}=\exp(-S)\sum_{n>2}\frac{S^n}{n!n} \tag{A19}$$

for any α and

$$\Gamma_{\xi\xi}^{10}=\frac{\exp(-S)}{2}\sum_{n>2}\frac{S^{n-1}}{n!(n-1)}[(n-S)^2+3n]\ , \tag{A20}$$

$$\Gamma_{\xi\xi}^{01}=\frac{\exp(-S)}{2}\sum_{n>2}\frac{S^{n-1}}{n!(n-1)}[3(n-S)^2+n]\ , \tag{A21}$$

$$\Gamma_{\eta\eta}^{10}=\Gamma_{\zeta\zeta}^{10}=\frac{\exp(-S)}{4}\sum_{n>2}\frac{S^{n-1}}{n!(n-1)}[5(n-S)^2+3n]\ , \tag{A22}$$

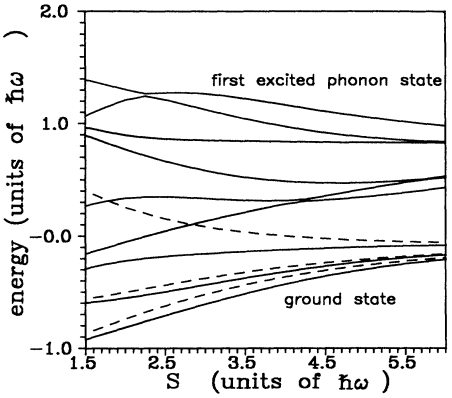

FIG. 11. Dependence of the energy structure of the zero- and one-phonon excited states of $^2T_2$ electronic manifold on the parameter S obtained for $\beta=200\ \text{cm}^{-1}$ and $\nu=500\ \text{cm}^{-1}$. Dashed curves represent energies of the zero vibronic states obtained by omitting the influence of the upper vibronic states (see text for detailed description). In both cases the phonon energy has been assumed to be $\hbar\omega=239\ \text{cm}^{-1}$.

$$\Gamma_{\eta\eta}^{01}=\Gamma_{\zeta\zeta}^{01}=\frac{\exp(-S)}{4}\sum_{n>2}\frac{S^{n-1}}{n!(n-1)}[3(n-S)^2+5n]\ . \tag{A23}$$

It is interesting to mention that if we restrict our problem to zero vibronic states, while the remaining excited vibronic states (including $|01\rangle$ and $|10\rangle$) are considered as a perturbation, our model is equivalent to that proposed by Macfarlane, Wong, and Sturge[23] and Bates and Bentley.[24] Thus the calculations performed under these assumptions give results identical to Ref. 23. One can reproduce the proper structure of the lowest three Kramers doublets related to the $^2T_2$ state, using quite large ν and β, assuming a medium Jahn-Teller effect. The results obtained for $\beta=200\ \text{cm}^{-1}$ and $\nu=500\ \text{cm}^{-1}$ are presented in Fig. 11 (dashed curves). A slight underestimation of the energy

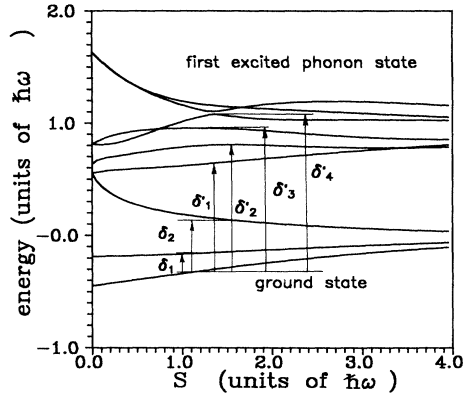

FIG. 12. Dependence of the energy structure of the zero- and one-phonon excited states of $^2T_2$ electronic manifold on the parameter S obtained for $\beta=80\ \text{cm}^{-1}$ and $\nu=200\ \text{cm}^{-1}$. The phonon energy has been assumed to be $\hbar\omega=239\ \text{cm}^{-1}$.

δ_1 with respect to δ_2 in comparison with the original result of Macfarlane, Wong, and Sturge[23] appears (see Fig. 12), since we have not considered the second-order correction to the off-diagonal matrix elements. However,if one performs the full calculations taking into account also the one-phonon excited states as described here, the resulting structure is quite different (see solid curves in Fig. 11). One can see that in the energy region under consideration ($\delta_2 \cong 0.5\hbar\omega$), for $S \equiv 3$, we have states which are originally related to the first phonon excitation. Actually, owing to the fact that the vibronic overlap integrals related to the wave function of the zero- and one-phonon states, and the one-phonon states of the different electronic manifolds, for large β and ν, are large, we have no well-separated phonon structure for the medium Jahn-Teller energy range. On the other hand, the analysis of the emission spectra of Ti^{3+}:sapphire yields a smaller Jahn-Teller effect than suggested by Macfarlane, Wong, and Sturge[23] (our prediction is $S \cong 1.4$). This is the reason for which it can be asserted that the spin-orbit interaction and the trigonal field distortion are much smaller than earlier calculations.[23] We have performed calculations using β on the order of 100 cm^{-1} and ν on the order of 200 cm^{-1}. The results for $\beta = 80$ cm^{-1} and $\nu = 200$ cm^{-1} are represented in Fig. 12. For $S = 1.4$ we have obtained $\delta_1 = 35$ cm^{-1} and $\delta_2 = 107$ cm^{-1}. These values are reasonable when compared with far-infrared spectroscopic data ($\delta_1 = 37$ cm^{-1} and $\delta_2 = 108$ cm^{-1}).[21,22] In addition, we have been able to predict quite accurately the structure of the first vibronic state. We have found three main components of the first vibronic state with energies: $\delta_1 = \hbar\omega + 38$ cm^{-1}, $\delta_2' = \hbar\omega + 73$ cm^{-1}, and $\delta_3' = \hbar\omega + 103$ cm^{-1}. The next higher components should give a broadband of energy $\delta_4' = \hbar\omega + 130 - 150$ cm^{-1} since they are almost degenerate. Such a structure has been experimentally observed by Gachter and Koningstein[8] in the low-temperature emission spectra of Ti^{3+}:sapphire. In general, one may conclude that the specific phonon structure of the $^2T_2$ state results mainly from the spin-orbit coupling and the existence of the trigonal crystal field. The nonlinear coupling with the lattice, if it exists, is rather small, and its contribution to the phonon structure of the ground state is negligible. Nevertheless, we considered nonlinear coupling in the main body of this paper since, albeit small, it can effectively control the nonradiative processes in the Ti^{3+} ion.

[1] P. Moulton, Opt. News **8**, 9 (1982).

[2] P. Moulton, Laser Focus **19**, 83 (1983).

[3] P. Albers, E. Stark, and G. Huber, J. Opt. Soc. Am. B **3**, 134 (1986).

[4] C. E. Ryvik and A. M. Buoncristiani, IEEE J. Quantum Electron. **QE-21**, 1619 (1985).

[5] P. F. Moulton, J. Opt. Soc. Am. B **3**, 125 (1986).

[6] See, for instance, S. Sugano, Y. Tanabe, and H. Kamimura, *Multiples of Transition Metal Ions in Crystals* (Academic, New York, 1970).

[7] D. S. McClure, J. Chem. **33**, 2757 (1962).

[8] B. F. Gachter and J. A. Koningstein, J. Chem. Phys. **60**, 2003 (1974).

[9] H. Bill, in *The Dynamical Jahn-Teller Effect in Localized States,* edited by Yu. E. Perlin and M. Wagner (North-Holland, New York, 1984), p. 703.

[10] M. Grinberg, A. Mandelis, and K. Fjeldsted, the following paper, Phys. Rev. B **48**, 5935 (1993).

[11] J. R. Englman, *The Jahn-Teller Effect in Molecules and Crystals* (Wiley-Interscience, New York, 1972).

[12] A. J. Wojtowicz, M. Kazmierczak, A. Lempicki, and R. H. Bartram, Opt. Soc. Am. **6**, 1106 (1989).

[13] H. K. Eigenmann, Ph.D. dissertation, Swiss Federal Institute of Technology, ETH, Zurich, Switzerland, 1970.

[14] G. F. Koster, J. O. Dimmock, R. G. Wheeler, and H. Statz, *Properties of Thirty-Two Point Groups* (MIT Press, Cambridge, MA, 1963).

[15] I. B. Biersuker, *Efect Jana-Tellera i Vibronnye Bzaimodeistvia v Sovremiennoj Chimii* (Nauka, Moscow, 1987) (in Russian).

[16] C. Cohen-Tannoudji, B. Diu, and F. Laloe, *Quantum Mechanics* (Wiley-Interscience, New York, 1977), Vol. 1.

[17] C. Manneback, Physica **17**, 1001 (1951).

[18] P. Albers and G. Huber, dissertation, Universitat Hamburg, FRG, 1985.

[19] M. D. Sturge, Phys. Rev. B **1**, 1005 (1970).

[20] F. S. Ham, Phys. Rev. **138**, A1727 (1965).

[21] E. D. Nelson, J. Y. Wong, and A. L. Schawlow, Phys. Rev. **156**, 298 (1967).

[22] R. R. Joyce and P. L. Richards, Phys. Rev. **179**, 375 (1969).

[23] R. M. Macfarlane, J. Y. Wong, and M. D. Sturge, Phys. Rev. **166**, 250 (1968).

[24] C. A. Bates and J. P. Bentley, J. Phys. C **2**, 1947 (1969).

[25] R. Rai, Phys. Status Solidi B **52**, 671 (1972).